A Land Surface Model (IAP94) for Climate Studies Part II: Implementation and Preliminary Results of Coupled Model with IAP GCM

Dai Yongjiu (戴永久), *Xue Feng* (薛 峰) and *Zeng Qingcun* (曾庆存)
Institute of Atmospheric Physics, Chinese Academy of Sciences, Beijing 100080
Received May 23, 1997; revised August 25, 1997

ABSTRACT

The Institute of Atmospheric Physics Land Surface Model (IAP94) has been incorporated into the IAP two-level atmospheric general circulation model (IAP GCM). Global and regional climatology averaged over the last 25 years of 100 year integrations from the IAP GCM with and without IAP94 ("bucket" scheme) is compared. The simulated results are also compared with the reanalysis data. Major findings are:

(1) The IAP GCM simulation without IAP94 has extensive regions of warmer than observed surface air temperatures, while the simulation with IAP94 very much improves the surface air temperature.

(2) The IAP GCM simulation with IAP94 gives improvement of the simulated precipitation pattern and intensity, especially the precipitation of East Asian summer monsoon and its intraseasonal migration of the rainbelts.

(3) In five selected typical regions, for most of the surface variables such as surface air temperature, precipitation, precipitation minus evaporation, net radiation, latent heat flux and sensible heat flux, the IAP GCM with IAP94 provides better simulations.

Key words: Land Surface Model, Coupled Model, Simulation

I. INTRODUCTION

The importance of land surface processes to short-period weather evolution and long-term climate variation has been increasingly recognized by the weather predicting and climate modelling community over the past 20 years. In order to improve the land-surface representations in the numerical weather predictions (NWPs) and in GCMs, the initiative of Dickinson (1984) with BATS and Sellers et al. (1986) with SiB was followed by many others who have taken part in the recent intercomparison project (PILPS) (Henderson-Sellers et al., 1996). Datasets describing soil and vegetation types at global scale were constructed for the use of GCMs (Matthews, 1985; Wilson and Henderson-Sellers, 1985; Dorman and Sellers, 1989; Sellers et al., 1996b).

Land surface processes partition the precipitation, evaporation, runoff, and temporary stores such as snow and soil moisture, and partition the net incident radiant energy, latent (evaporation) and sensible heat loss. The land surface also alters radiative fluxes through the surface albedo, soil moisture and surface temperature. Momentum exchange between the atmosphere and land surface is determined by the representation of surface drag. In the 1970s and early 1980s, land surface processes in the model were represented by prescribed albedo, roughness lengths and a simple "bucket" hydrology. Such models have been widely used in the weather and climate simulations. More recently the improved land surface parameterizations consist of representations of leaves, roots, multiple soil types and layers,

the dependence of albedo, roughness and stomatal conductance on the type of vegetation and its canopy geometry, and carbon uptake and respiration. Nowadays, most of the GCMs with the improved land surface processes, however, are still experimental versions instead of standard (operational) versions. This is due to the fact that the long-term climate equilibrium integrations and the quantitative model evaluations can be made only by observational data which are primarily necessary, but still very incomplete. In addition, this is also the crucial prerequisite for all meaningful sensitivity experiments on the continental climate and land-surface states.

Due to a long 'memory' time for the soil moisture and the deep soil layer temperature which undergoes a seasonal variation (Ye et al., 1984; Yang et al., 1995a), and current coupled GCM run can be made only by using some incomplete surface variables data, starting from initial conditions which consist of some observed land surface variables and some initial variables usually taken from the climate equilibrium. The state of the coupled system after adjustment is then commonly used to initiate both the control runs and the climate change experiments. Until now, only a few climate modelling groups have published their results of the long-term climate equilibrium integrations by GCMs with their advanced land-surface parameterization schemes (e.g., Yang et al., 1995; Thompson and Pollard, 1995; Mahfouf et al., 1995; Randall et al., 1996; Bonan, 1996). All of these experiments have demonstrated that more realistic descriptions of land surface processes in incorporation with GCM lead to more realistic and accurate calculations of the land surface-atmosphere fluxes, surface temperature and soil moisture.

The major objectives of the present work are: 1) to assess the performance of a coupled system consisting of IAP AGCM and IAP land surface model (IAP94); 2) to check the stability of this coupled model in long-term integration and 3) to study the impact of the land surface processes on the climate. Two 100 year runs have been made by us, one is the control run (without IAP94, hereafter referred to as CTL-GCM), and another is made by using the Land Surface Model IAP94 coupled to AGCM (hereafter referred to as IAP94-GCM). The prescribed climatological sea surface temperatures (SSTs) and sea ice are used in both simulations, because our purpose is to pick up the importance of land surface processes.

The IAP94 formulation and its validation in off-line experiments have been described in Part I of our paper (Dai and Zeng, 1997). The purpose of Part II describes only the climate simulation results in some detail. It is organized as follows. In Section 2, we provide a short summary of the IAP two-level AGCM and IAP94, the information of global vegetation and soil, and the design of experiment. In Section 3, the results of the last 25 years of a fully equilibrated 100 year run are compared with a control run and with available observed climatology. The summary and conclusions are presented in Section 4.

II. MODEL DESCRIPTION AND EXPERIMENT DESIGN

1. *IAP AGCM*

In the present study, the IAP AGCM, namely the first generation of IAP AGCM is adopted for saving computations. It is a grid-point model with a grid spacing of 4° of latitude by 5° of longitude with two interior tropospheric levels (no stratospheric level is simulated). A detailed description of the model can be found in Zeng et al. (1989), its main aspects are briefly summarized below.

The model is formulated in the vertical σ-coordinate system given by $\sigma = (p - p_T) / (p_s - p_T)$, where p is pressure, p_T the constant pressure at the top of the model atmosphere (200 hPa), and p_s surface pressure. The tropospheric prognostic variables of the model are the horizontal velocity, the temperature, and the water vapor mixing ratio; each of these is carried at the two, equally spaced interior tropospheric levels $\sigma = 1/4$ and $\sigma = 3/4$. The surface pressure p_s as well as the surface temperature, the ground wetness, and the snow amount are also prognostic variables. In addition to these variables, certain quantities are determined diagnostically.

The dynamic framework of the model is, to some extent, different from other model in the world. The major different points are the following: (1) The departures of temperature T', geopotential φ' and surface pressure p' from the "standards" are introduced to cancel automatically the large truncation errors in the mountain and complicated topography regions; (2) The coordinates and variables are transformed in such a way that leads the energy equation to a very compact form and the grid to more flexible arrangement; (3) The computational scheme exactly keeps the "available" energy conservation (in the absence of sources and sink), and is free from computational modes; (4) The formulation and calculation of boundary terms or boundary conditions at the interfaces of atmosphere–ocean and atmosphere–land are physically consistent.

The model has a comprehensive package of physical parameterizations that are performed once each simulated hour. The parameterization of cumulus convection is based on the scheme developed by Arakawa et al. (1969). Three types of cumulus are simulated: the middle-level convection, the penetrating convection and the low-level convection. The cumulus mass flux for middle-level and penetrating convection is determined by assuming that the instability associated with these forms of convection is removed within a time scale (for one hour).

Cloudiness in the model is parameterized as a result of both large-scale and convective motions. Large-scale cloudiness occurs when the relative humidity exceeds 90% in the lower layer and 100% in the upper layer respectively, while the cloudiness resulting from convective motion is always overcast; the total cloudiness refers to all coexisting cloud types. Each type of simulated cloud has an assigned thickness and representative optical properties and interacts with the transfer of both solar and long-wave radiation; the liquid content in cloud is neglected.

The diabatic heating rate at the upper level contains the absorption of solar radiation in the upper layer (dependent on the predicted clouds and water vapor mixing ratio) and the release of the latent heat if condensation of water vapor occurs. The heating rate at lower level contains the same quantities but for the upper layer and, in addition, includes the sensible heat flux from the bottom surface. The total condensation rate at both model levels is the sum of that from both large-scale and convective-scale processes, the latter of which results from the model's convective adjustments required to maintain a stable lapse rate. The total precipitation at the surface is equal to the net difference between the condensation and the evaporation from falling precipitation in the atmospheric column.

Solar radiation is calculated by the modified delta-Eddington model of Cess (Cess, 1985; Cess et al., 1985; Cess and Potter, 1987) in which the atmospheric Rayleigh scattering and the effects of scattering, and absorption by cloud droplets, water vapor, ozone and aerosols are incorporated. Solar radiation is absorbed above the tropopause (200 hPa) by ozone, water vapor and cloud droplets, below the tropopause by water vapor, aerosols and cloud droplets. The solar spectrum is divided at 0.5 μm and 0.9 μm into three wavelength intervals

(ultraviolet, visual and near-infrared bands). Long-wave radiation is parameterized following the scheme developed by Katayama (1972). Absorption and emission are due to water vapor and carbon dioxide, expressed in terms of two frequency-weighted mean transmission functions and a bulk transmission function. Clouds are treated as grey body radiators with emissivities of 0.5 for cirrus clouds and 1.0 otherwise. The total ozone amount is prescribed once each day by linear interpolation from the monthly zonal-mean total ozone data of Dutsh (1971), and carbon dioxide mixing ratio is assumed to be constant (0.000489).

The surface boundary layer in the model is parameterized as a constant flux layer of undefined thickness. The surface stress, sensible heat and evaporation fluxes are parameterized according to the bulk aerodynamic method, with effective vertical diffusion coefficient dependent on low-level stratification, and the effect of topographical elevation. The surface air temperature is found by equating the surface flux of sensible heat as parameterized in term of K-theory. The ground temperature is determined by the heat balance equation for ground, assuming a bulk thermal heat capacity with the diurnal frequency. The ground wetness is determined by the ground water budget equation that accounts for rainfall, snowmelt, surface evaporation and surface runoff (bucket hydrology). Of course the calculation of the surface temperature and ground temperature as well as the soil moisture and hydrology is changed when the IAP94 is coupled with the GCM).

Together with a large number of other modelling groups, the IAP two-level AGCM has also taken part in AMIP investigations (Gates, 1992). The model results are evaluated against a number of climatological datasets (Xue and Zeng, 1997). The model has also been widely applied in short-term climate prediction experiments in China (Zeng et al., 1994).

2. *IAP Land-Surface Model (IAP94)*

The formulation of IAP land surface model (IAP94) has been described in detail in Part I. Here we briefly review the structure and the atmospheric boundary conditions of the model, and the parameterization of grid-averaged fluxes and albedo.

This model is a rather comprehensive one with detailed description for the processes of vegetation, snow and soil. Particular attention has been paid to the cases with three water phases in the surface media. As in other advanced land-surface parameterization schemes, canopy in IAP94 is explicitly parameterized as a single layer. The water storage on leaves is determined from the balance of the intercepted precipitation and the evaporation of the retained water. The foliage temperature is obtained from the solution of a canopy energy budget equation taking into account of the exchanges above and below the canopy. The air temperature and humidity within canopy space are predicted by the sensible heat and water vapor balance equations with the assumption of zero capacity for heat and water vapor.

The soil column is discretized into three layers, i.e., (1) surface layer, from which soil water can be directly evaporated into the atmosphere, and the temperature undergoes a diurnal variation; (2) intermediate layer, it is the vegetation rooting zone, but in which the root may not exceed the bottom; (3) deep layer, where the transfer of water is governed only by gravitational drainage and hydraulic diffusion, and the temperature undergoes a seasonal and annual variation. In the presence of snow on the ground, the water and heat balance of snow media should be considered when the depth of snow accumulation reaches 1 cm, but it can be combined with the surface soil layer otherwise. With accumulating or ablating, the snow layer is subdivided or combined simultaneously at the end of each time step, the maximum number of discretization layers of snow is limited to 3. The governing equations for the temperature and water content are based on the conservation of energy and mass within each

soil or snow layer.

The upper boundary conditions for IAP94 are as follows: air temperature, humidity and wind speed of the lower atmospheric model layer, incident solar and atmospheric radiation and solar zenith angle, and the precipitation rate.

IAP94 permits limited heterogeneity at the land surface so that bare soil, vegetation and snow cover can coexist simultaneously in a grid square. Each grid square is divided into four separate subareas to the maximum, bare soil, snow cover, vegetation cover and snow-and-vegetation cover. They are used to partition the total surface evapotranspiration, and to estimate the averaged surface albedo. The grid-averaged evapotranspiration flux is parameterized by the weighted sum of four components (evaporation from bare soil, foliage transpiration and interception loss, sublimation from snow cover). In the present version of IAP94, the ground surface temperature is assumed equivalent to the coexistence case of bare soil and snow cover, and the grid-averaged sensible heat flux is parameterized by the weighted sum of two components (from the non-vegetated ground, and the vegetation canopy). The grid-averaged albedo is calculated by the weighted sum of four components.

3. *Vegetation and Soil Information*

As mentioned in the above sub-section, the surface atmospheric boundary layer in the IAP GCM is parameterized as a constant flux layer, and the physical package is called at each simulated hour. When the IAP94 is coupled with IAP GCM, what we should make is to replace the CTL-GCM surface flux scheme by IAP94 formulations, and introduce new global data on the categories of land cover and the assignment of the characteristic parameters.

In CTL-GCM, the world's vegetation is classified into four categories (1-woodland and grass cultivation; 2-forest; 3-steppe and grassland; 4-tundra, mountains and Arctic flora). This classification is too simple for assigning parameters reasonably to represent the morphological and physiological characteristics of the vegetation community. The world's soil is taken as identical in CTL-GCM, which takes the form of bucket hydrology.

In IAP94-GCM, the SiB global archive of land cover established by Dorman and Sellers (1989) is used, in which twelve classes of land types are defined, and each $4^\circ \times 5^\circ$ grid element is assigned. In SiB archive, most of grids over China are assigned as bare soil (desert), it greatly misrepresents the land cover types over this region. According to "Vegetation of China", we have assigned a modified distribution for China region. The time-independent and time-varying biome parameters associated with each of vegetation types are taken from Dorman and Sellers (1989), Xue et al. (1991), and Dickinson (1986).

Wilson and Henderson-Sellers (1985) classified soil color, texture, and drainage using the FAO Soil Map of the World as the soil data source. Soil information is archived at $1^\circ \times 1^\circ$ resolution in three color classes, three texture classes, and three drainage classes. A soil type archive has been constructed from these data and transferred into the $4^\circ \times 5^\circ$ model grids, but partly modified for China region according to "Soil of China" (Li et al., 1988). According to the methodologies of BATS used to define the global distribution of soil types and to attribute it into climate models, eight color classes (light-dark), twelve texture classes, ranging from 1 = very coarse (sand) to 12 = very fine (heavy clay) are assigned by averaging the texture from the $1^\circ \times 1^\circ$ data set. Soil properties associated with the twelve texture classes, dry and saturated albedos in two wavelength regions associated with the eight color classes are from the BATS assignment (Dickinson et al., 1986) and other scientific literatures.

4. *Experimental Design*

Two 100-yr simulations have been made with IAP GCM. One simulation was made by using of IAP94 to represent the complicated land-surface (IAP94-GCM), while another was made by using of a "bucket hydrology" model (CTL-GCM). The atmospheric variables of the control run (by using CTL-GCM) and the coupled run (by using IAP94 GCM) were initialized using 1 January, with the same initial states. For the run coupled with IAP94, the initial ground temperature of each soil layer was taken as equal to the single initial ground surface temperature as in the control run. The canopy water storage was initially equal to zero everywhere. the initial soil moisture is the same value in each soil layer as in the control run. If the soil temperatures are less than the freezing temperature 273.15K, the soil water is initialized as ice grain. In the control run, the initial surface field provides only the water equivalent of snow, while the initial snow thickness is required for running IAP94-GCM. In order to obtain the initial snow thickness, we arbitrarily set the snow density as 300 kg / m^3. When the initial snow thickness is greater than 1 cm, the snow layers are initiated according to the rule of IAP94 snow layer division. The effect of the glaciers is treated like snow cover, the volume fraction of frozen water in three ice layers is taken as that in which ice density is equal to 917 kg / m^3, the thermal properties of ice are used for each layer, and no infiltration of water is allowed at the surface.

The SST and sea ice in these two experiments are taken from the climatological data averaged during the period of 1979-1988.

III. RESULTS AND COMPARISON WITH A CONTROL RUN AND WITH OBSERVATIONS

In this section, the simulations generated by the IAP94-GCM and CTL-GCM are compared with each other and with the observed climatologies. First of all, analyses of some primary variables for describing global climate are presented. Secondly, the impact of IAP94 on surface climatology and fluxes are examined in the selected five regions.

All simulated fields are the monthly means averaged over the last 25 years of a fully equilibrated 100 year run. We compared the model's climatology with that of NCEP / NCAR reanalysis (hereafter referred to as reanalysis) for 11 years (1982-1992) of monthly climatological data (Kalnay et al., 1996).

1. *Simulation of Global Seasonal Mean Climate*

(1) Surface air temperature

The geographic distributions of surface air temperature in the DJF and JJA seasons (winter and summer) simulated by IAP94 and CTL GCM are shown in Fig.1, together with the observations. Overall, both models have successfully simulated the large-scale features of the observed surface air temperature, for example, cold centers in Siberia, Greenland and Antarctic in winter and high temperature region extending from North Africa to South Asia in summer are well reproduced by the models. Comparison further shows that the control simulation is greatly warmer than the observed over continent, examples are the Sahara and Saudi-Arab deserts, South and East Asia and Antarctic, with the overestimations by 5°C to 10°C. This model's anomalous feature is contrary to the high resolution models' (Randall et al., 1996). In general, IAP94-GCM leads to a general and fairly dramatic improvement of the simulation of surface air temperature and thus gives a more realistic distribution. This result

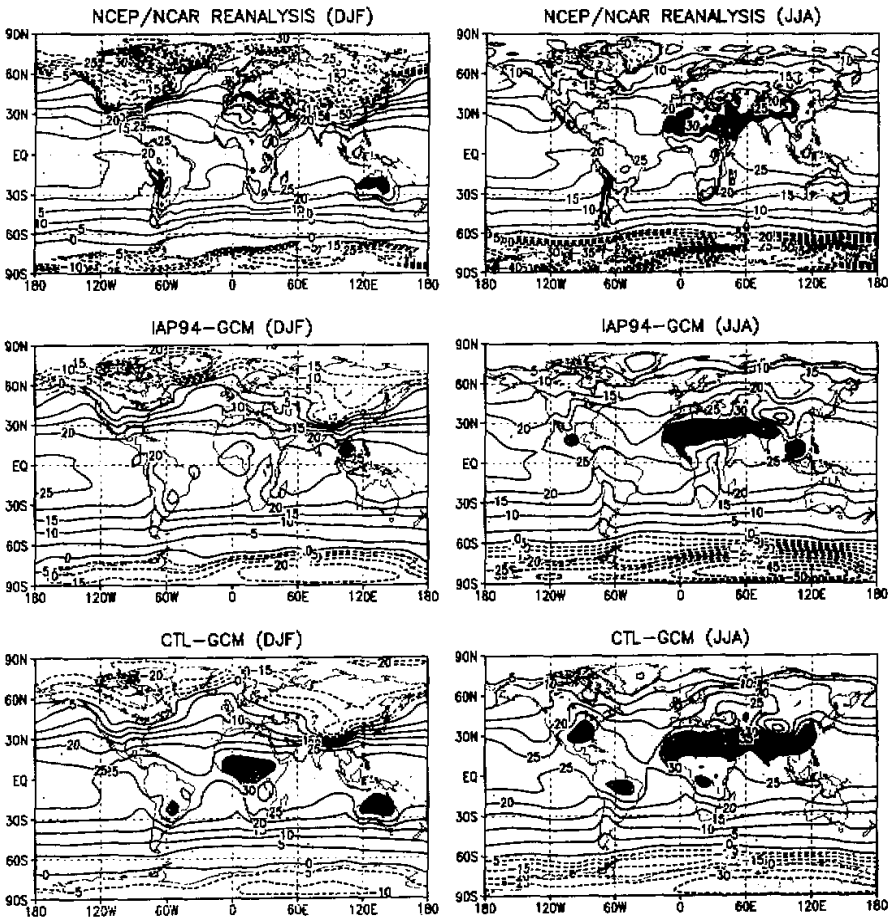

Fig. 1. Observed and simulated global geographical distributions of *DJF* and *JJA* surface air temperature (°C). Dark-shaded areas are the regions where temperature great than 30°C, and grey-shaded areas are the regions where temperture less than -30°C.

shows that the incorporation of a detailed land surface model into a GCM is necessary to the simulation of surface air temperature.

(2) Sea level pressure

Fig.2 gives the December-February and June-August distributions of the observed as well as of the IAP94-GCM and CTL-GCM simulated sea level pressure fields. In DJF, the Antarctic circumpolar low and the three subtropical anticyclones in the Southern Hemisphere are correctly reproduced by both IAP94-GCM and CTL-GCM, but the IAP94-GCM simulation is better. In the Northern Hemisphere, in comparison with the reanalysis, the Siberian anticyclone is slightly weaker, and the Aleutian and Icelandic lows are deeper and result in an overestimation of the westerlies in the mid-latitudes in both IAP94-GCM and CTL-GCM, but the IAP94-GCM simulation is also better.

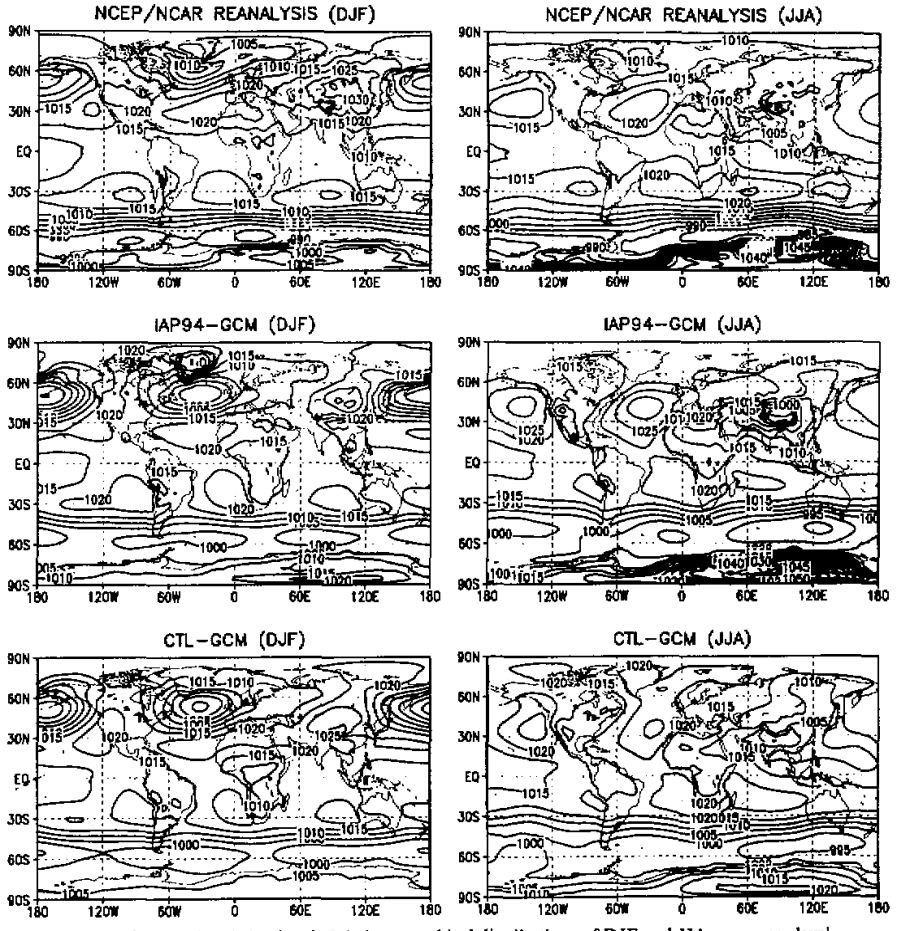

Fig. 2. Observed and simulated global geographical distributions of DJF and JJA mean sea-level pressure (hPa).

In JJA, the 40°S–60°S cyclonic belt simulated in the CTL–GCM is in good agreement with the reanalysis climatology. This belt is also well simulated by IAP94–GCM, however, it is slightly northwards than that in the reanalysis. The two Northern Hemisphere anticyclones (subtropic highs) are correctly simulated in general by both the IAP94–GCM and CTL GCM except for a slightly northward of the location. The simulation by IAP94–GCM is better except for overestimation of the intensity. Regarding the monsoon circulation, the low pressures over Southwest Asia are well reproduced by both models. The last point will be further discussed in the next paper.

The low-pressure belt around Antarctica, which is not deep enough and spreads too far equatorward. Boville (1991) has found similar performance in the NCAR CCM1 general circulation model and described the improvements obtained at higher spatial resolutions.

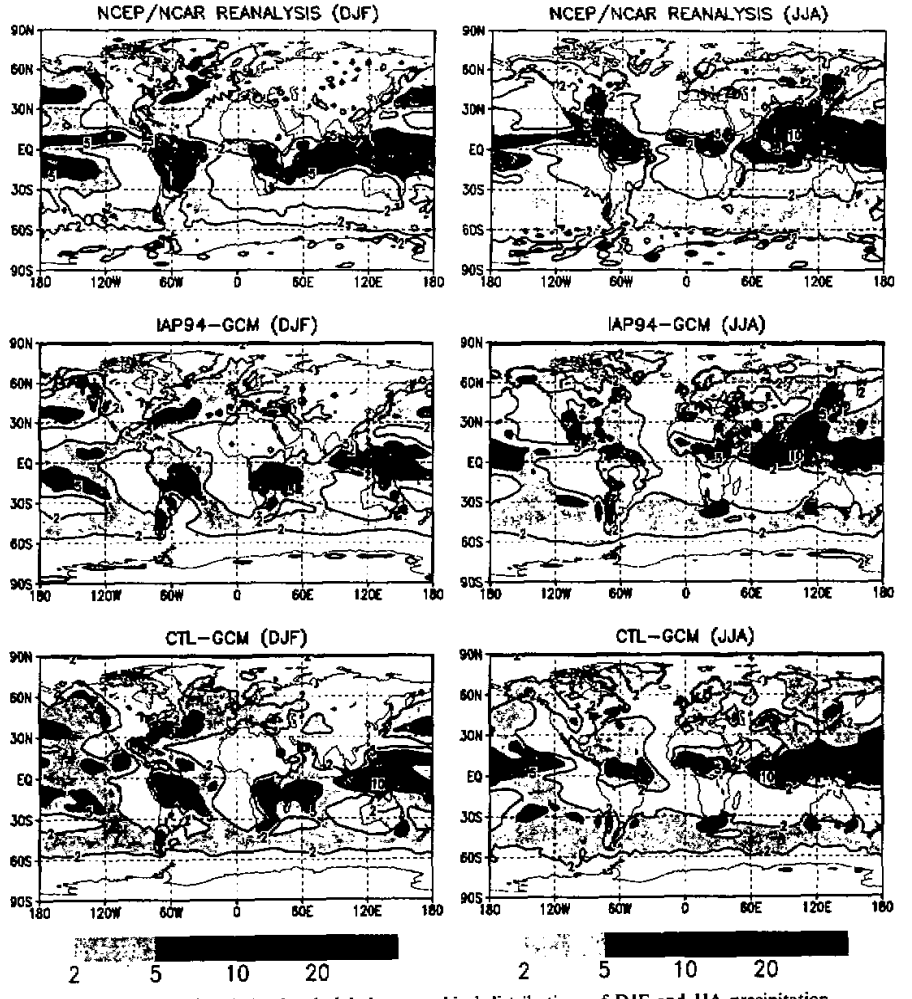

Fig. 3. Observed and simulated global geographical distributions of DJF and JJA precipitation rate (mm / day). Contours are plotted at 2.5, 10 and 20 mm per day.

(3) Precipitation rate

Fig.3 gives the December–February and June–August distributions of the IAP94–GCM and CTL–GCM simulated as well as the observed precipitation maps. In the observation, during December–February there is a strong tropical rain belt located in the equatorial region and extended to about 15°S, two rain regions respectively in the Eastern and Western Hemisphere in the Northern Hemisphere along the storm tracks, and one rain belt in the middle latitude of the Southern Hemisphere are well simulated by both models, but the IAP94–GCM simulation is better, especially the rain intensity in the tropical belt. During June–August, the rain belts associated with the storm tracks in the westerlies and the rain belt located in the tropical region and extended to the Asian monsoon rain regions all appear in the observation and both simulations. However, the IAP94–GCM very much improves the simulation of

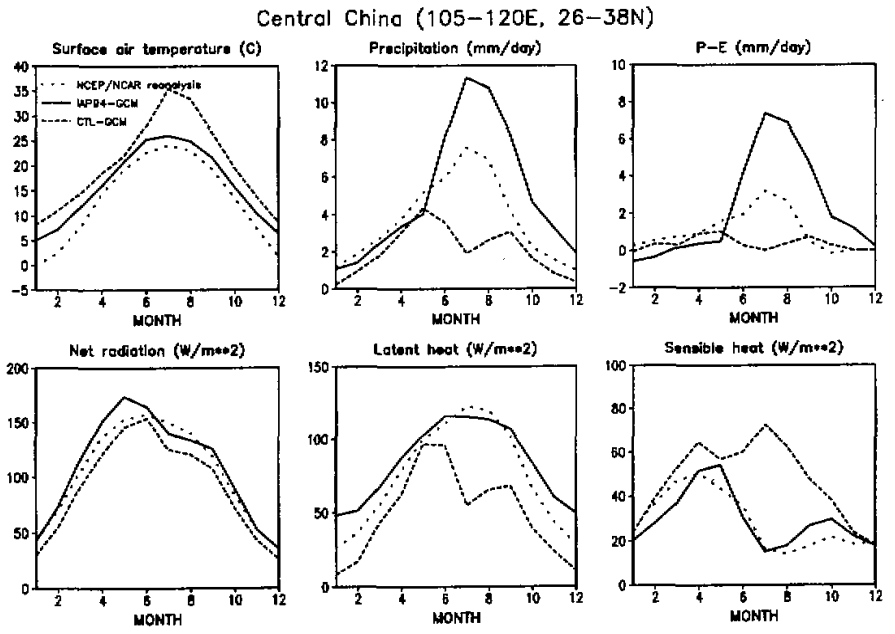

Fig. 4. Monthly averaged surface air temperature, precipitation, precipitation minus evaporation, net radiation, latent heat flux, and sensible heat flux for region of Central China (26°–38°N, 105°–120°E).

Asian monsoon rain belt both in the pattern similarity and in the intensity and thus is in good agreement with the observation. Especially, the Asian summer monsoon rain belt is extended from India Peninsular, the South China Sea and the vicinity of Philippines and the Warm Pool region, to the eastern coast area of Asian continent and Japan. This picture very well resembles the observation.

2. *Simulation of Regional Surface Climatology*

The impact of IAP94 on surface climatology and fluxes will be examined by selecting four geographic regions: Central China (cultivation), Tibetan Plateau (snow and semi-desert), East Siberia (forest and frozen soil), Central Sahel (desert), Amazon basin (rainforest). Monthly and regional averaged surface air temperature, precipitation, precipitation minus evaporation (P–E), net radiation, latent heat flux, and sensible heat flux are compared between simulation and the reanalysis.

(1) Central China

Fig.4 shows the monthly averaged surface air temperature, precipitation, precipitation minus evaporation (P–E), net radiation, latent heat flux and sensible heat flux over Central China (26°–38°N, 105°–120°E). Although both models give a higher surface air temperature than the reanalysis throughout the year, the simulation of IAP94–GCM is closer to observation. Precipitation is also well simulated by IAP94–GCM except for rather high amount in rainy season. However, CTL–GCM simulation gives too warmer summer and insufficient precipitation. The simulation of P–E is similar to precipitation, i.e., the IAP94–GCM

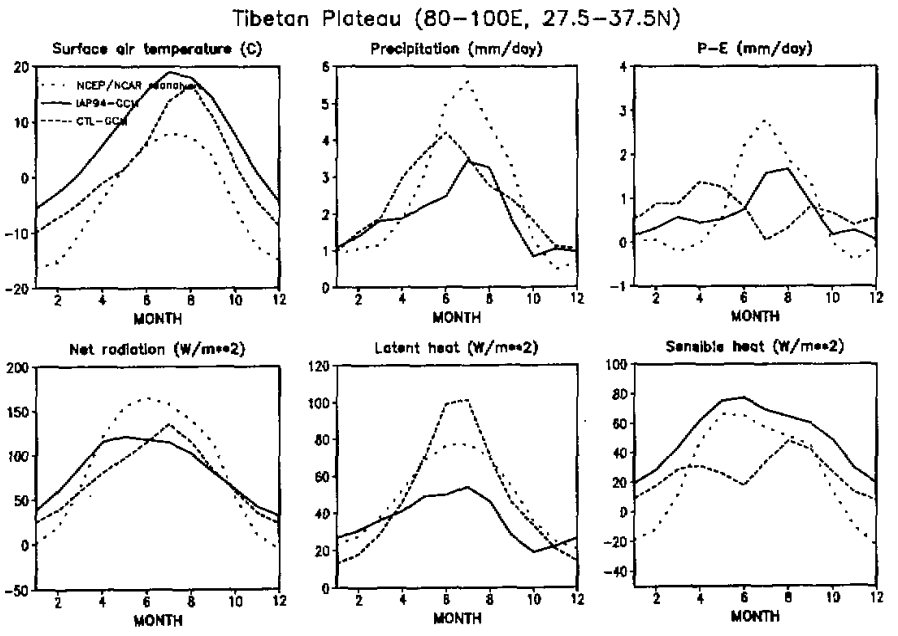

Fig. 5. Same as fig.4, but for the Tibetan Plateau (28°–38°N, 80°–100°E).

gives more realistic simulation of P–E, but the value is larger than the reanalysis during summer (Note, that there are some uncertainties in both measurement and simulation of evaporation). The net radiation simulated by two models is well consistent with the reanalysis. The latent heat flux simulated by IAP94–GCM is similar to the reanalysis, but slightly higher in winter. While CTL–GCM underestimates latent heat throughout the year, especially, latent heat decreases in summer due to a small precipitation. The sensible heat flux simulated by IAP94–GCM is consistent with the reanalysis, but CTL–GCM largely overestimates the sensible heat flux due to a less latent heat partitioning the high solar heating in summer.

(2) Tibetan Plateau

Fig. 5 is the same as Fig.4 but for the Tibetan Plateau (28°–38°N, 80°–100°E). IAP94–GCM overestimates the surface air temperature by 8°C in comparison with the observation. While, the CTL–GCM gives a less overestimation of the surface air temperature. Precipitation is underestimated by both IAP94–GCM and CTL–GCM during the period of May to September, however, IAP94–GCM has a closer P–E to the reanalysis than CTL–GCM due to smaller latent heat flux. Compared with the reanalysis, both models have a slightly higher net radiation during the Tibetan Plateau colder season but have lower values in summer (the time of the peak value is different, IAP94–GCM in April–May, CTL–GCM in July, and the reanalysis in June). From April to November, IAP94–GCM largely underestimates the latent heat flux, but the CTL–GCM is similar to the reanalysis. For sensible heat simulation, both models provide a positive contribution to the atmosphere, so that there exists a heat source throughout the year, but IAP94–GCM has a more sensible heat than CTL–GCM from March to September, and thus is closer to the reanalysis.

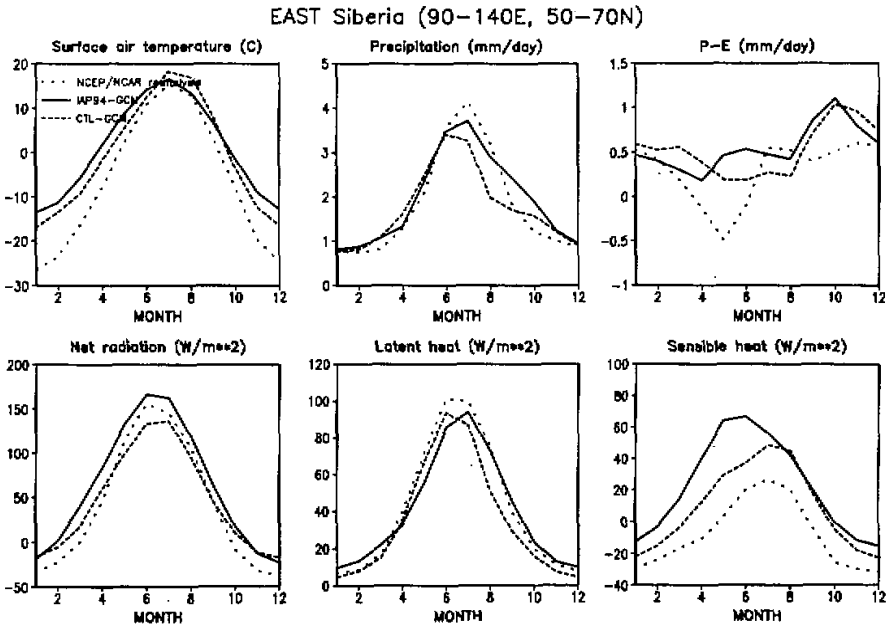

Fig. 6. Same as Fig.4, but for East Siberia (50°–70°N, 90°–140°E).

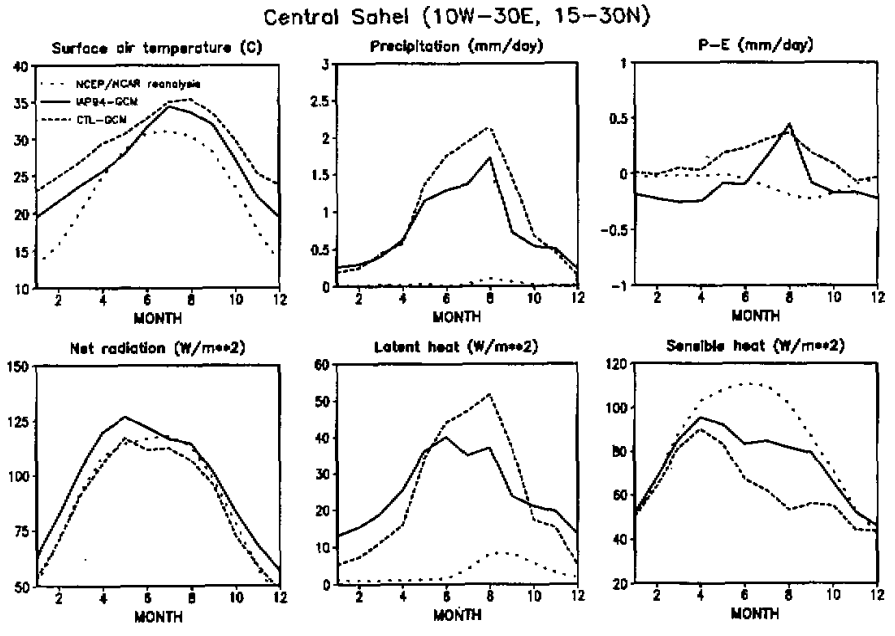

Fig. 7. Same as Fig. 4, but for Central Sahel (15°–30°N, 10°W–30°E).

(3) East siberia

Fig. 6 is the same as Fig.4 but for East Siberia (50°–70°N, 90°–140°E). Both models overestimate the surface air temperature by a similar amount except for June to August. During this period, IAP94–GCM gives a correct simulation. Precipitation is reasonably simulated by both models compared to the observation. The simulated P–E by the two models does differ from that of the reanalysis in the snow melting season (April–May), during this period the simulated P–E is positive instead of negative in the reanalysis. Net radiation and latent heat flux are similar for both models and the reanalysis. Both models have a more sensible heat than observation, however, IAP94–GCM aggravates this bias in spring and early summer.

(4) Central sahel

Fig.7 is the same as Fig.4 but for Central Sahel (15°–30°N, 10°W–30°E). Both models have a warmer surface temperature bias throughout the year, but IAP94–GCM is statistically colder than CTL–GCM, hence the simulated temperature by IAP94–GCM is closer to observations. IAP94–GCM and CTL–GCM, especially the CTL–GCM, largely overestimate precipitation and latent heat flux throughout the year. As a result, more rainfall stores in soil and then provides to evaporation, the latent heat flux is higher than that of the reanalysis. It is noticeable that IAP94–GCM P–E is in deficit except in July and August. P–E in the reanalysis is negative but in the CTL–GCM is positive throughout the year. Both models well simulate net radiation. The simulated sensible heat flux by IAP94–GCM is close to observations, but the CTL–GCM largely overestimates the sensible heat flux.

(5) Amazon basin

Fig.8 is the same as Fig.4 but for Amazon Basin (12°S –0°, 70°–50°W). The observed surface air temperature shows a slight variation throughout the year, IAP94–GCM reproduces this observed variation, but underestimate it by about 3°C. While CTL–GCM poorly reproduces this picture, instead, a large unrealistic warming occurs from May to September in the simulation. Both models underestimate precipitation and P–E, but clearly reproduce the variation of the dry and rainy seasons and the annual cycle of P–E. The seasonal variation of net radiation, latent and sensible heat fluxes are well simulated by IAP94–GCM in comparison with the reanalysis, except for overestimation of net radiation and sensible heat and underestimation of latent heat.

In summary, IAP94 GCM has a better performance in simulating the regional climate for all the selected five regions than the previous model, the most striking improvements are found in Central China, where all the simulated variables by the coupled model are much more accurate than the old one. The rather large bias is found in Amason region, where the bias is systematic and larger than that in other regions. Besides, the simulated precipitation in Sahel region is also systematically larger than the observed one although the simulation by IAP94 GCM seems better.

IV. SUMMARY

The IAP land surface model (IAP94) has been successfully coupled to IAP AGCM as an operational, standard component of the coupled model. The coupled GCM makes a more realistic simulation of the global distribution of surface air temperature, and an improved simulation of sea surface pressure and the precipitation, especially, the improvement of precipitation pattern and intensity of Asian monsoon is very significant. Besides, in the five selected regions representing typical different surface regimes, for most of some important surface variables such as surface air temperature, precipitation, precipitation minus evaporation,

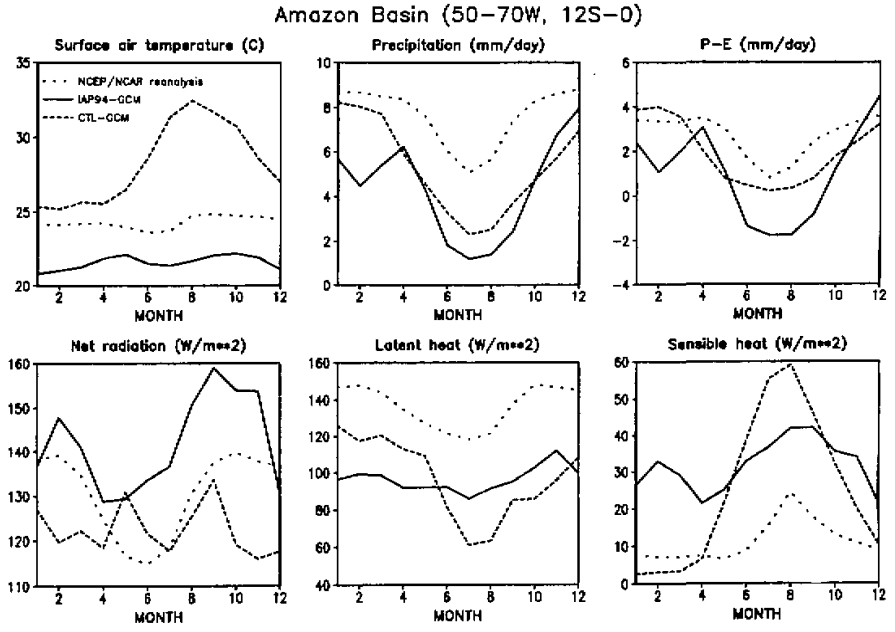

Fig. 8. Same as Fig. 4, but for Amazon basin (10°S–0°, 70°–50°W).

net radiation, latent heat flux and sensible heat flux, the coupled model provides improved and more realistic simulations. Therefore, it can be concluded that the incorporation of an advanced land surface model into AGCM is necessary for climate simulation in both global and regional scale. In particular, due to the improvement of simulation in East Asian monsoon region, IAP94 GCM may open a new prospect to the short-range climate prediction in China following our pioneering work (Zeng et al., 1997).

REFERENCES

Arakawa A., Katayama A., and Y. Mintz (1969), Numerical simulation of the general circulation of the atmosphere, *Proceedings of the WMO / IUGG Symposium on Numerical Weather Prediction*, Tokyo, Japan Meteor. Agency, pp. IV-7 to IV-8-12.

Bonan G.B. (1996), The NCAR land surface model (LSM version 1.0) coupled to the NCAR Community Climate Model, NCAR Tech. Note, NCAR / TN-429+STR, 171 pp.

Boville B.A. (1991), Sensitivity of simulated climate to model resolution, *J. Climate*, **4**: 469-485.

Cess R.D. (1985), Nuclear war: Illustrative effects of atmospheric smoke and dust upon solar radiation, *Climate Change*, **7**: 237-251.

Cess R.D. and G.L. Potter (1987), Exploratory studies of cloud radiation forcing with a general circulation model, *Tellus*, **39A**: 460-473.

Cess R.D., Potter G.L., Ghan S.J., and W.L. Gates (1985), The climate effects of large injections of atmospheric smoke and dust: A study of climate feedback mechanisms with one- and three-dimensional climate models, *J. Geophys. Res.*, **90**: 12937-12950.

Dai Y.J. and Zeng Q.C. (1997), A land surface model (IAP94) for climate studies, Part I: Formulation and validation in off-line experiments, *Advances in Atmos. Sci.*, **14**: 433-460.

Dickinson R.E. (1984), Modelling evapotranspiration for three-dimensional global climate models, *Climate Processes and climate Sensitivity. JE Hanson and T Takahashi, Eds., Geophys. Monogr.*, Amer. Geophys. Union., **29**: 58-72.

Dickinson R.E., A. Henderson-Sellers, Kennedy P.J., and M.F. Wilson (1986), Biosphere atmosphere transfer scheme (BATS) for NCAR Community Climate Model, NCAR Tech. Note NCAR / TN-275+STR, 69 pp.

Dickinson R.E., A. Henderson-Sellers, Kennedy P.J., and M.F. Wilson (1993), Biosphere atmosphere transfer scheme (BATS) version 1e as coupled to for Community Climate Model, NCAR Tech. Note NCAR / TN-378+STR, 72 pp.

Dorman J.L and P.J. Sellers (1989), A global climatology of albedo, roughness length and stomatal resistance for atmospheric general circulation models as represented by the simple biosphere model (SiB), *J. Appl. Meteor.*, **28**: 833-855.

Dutsh H.U. (1971), Photochemistry of atmospheric ozone, *Advances in Geophys.*, **15**: 219-322.

Gates W.L. (1992), The atmospheric model intercomparison project, *Bull. Amer. Meteor. Soc.*, **73**: 1962-1970.

Henderson-Sellers A., McGuffie K., and A.J. Pitman (1996), The Project for Intercomparison of Land-surface Parameterization Schemes (PILPS): 1992 to 1995, *Clim. Dyn.*, **12**: 849-859.

Kalnay E., coauthors (1996), The NCEP / NCAR 40-year reanalysis project, *Bull. Amer. Meteor. Soc.*, **77**: 437-471.

Katayama A. (1972), A simplified scheme for computing radiative transfer in the troposphere, Tech Rep No.6, Department of Meteorology, University of California, Los Angeles, CA, 77 pp.

Li Q.K., coauthor (1988), Soil of China. Science Press, Beijing, PP157 (in Chinese).

Mahfouf J.F., Manzi A.O., Noilhan J., Giordani H., and M. Deque (1995), The land surface scheme ISBA within the Meteo-France climate model ARPEGE. Part I: Implementation and preliminary results, *J. Clim.*, **8**: 2041-2057.

Map of Vegetation of China, Hou X.Y. ed., China Cartological Press, 1979, pp 253 (in Chinese).

Matthew (1983), Global vegetation and land use: New high-resolution data bases for climate studies, *J. Appl. Meteorl.*, **22**: 474-487.

Randall D.A., Dazlich D.A., Zhang C., Denning A.S., Sellers P.J., Tucker C.J., Bounoua L., Berry J.A., Collatz G.J., Field G.B., Los S.O., Justice C.O., and I. Fung (1996), A revised land surface parameterization (SiB2) for atmospheric GCMs, Part III: The greening of the Colorado State University general circulation model, *J. Clim.*, **9**: 738-763.

Sellers P.J., Mintz Y., Sud Y.C., and A. Dalcher (1986), A simple biosphere model (SiB) for use within general circulation models, *J. Atmos. Sci.*, **43**: 505-531.

Sellers P.J., Sietse O.L., Tucker C.J., Justice C.O., Dazlich D.A., Collatz G.J., and D.A. Randall (1996b), A revised land surface parameterization (SiB2) for atmospheric GCMs. Part II: The generation of global fields of terrestrial biophysical parameters from satellite data, *J. Clim.*, **9**: 706-737.

Thompson S.L. and D. Pollard (1995), A global climate model (GENESIS) with a land surface transfer scheme (LSX). Part I: Present climate simulation, *J. Clim.*, **8**: 732-761.

Wilson M.F. and A. Henderson-Sellers (1985), A global archive of land cover and soil data for use in general circulation climate models, *J. Clima.*, **5**: 119-143.

Xue F. and Q.C. Zeng (1997), Simulation of January and July monthly mean climate and validation of IAP GCM, Climatic and Environmental Research (to be published).

Xue Y.K., Sellers P.J., Kinter J.L., and J. Shukla (1991), A simplified biosphere model for global climate studies, *J. Clim.*, **4**: 345-364.

Yang Z.L., Dickinson R.E., Henderson-Sellers A., and A.J. Pitman (1995c), Preliminary study of spin-up processes in land-surface models with the first stage data of PILPS Phase 1(a), *J. Geophys. Res.*, **100(D8)**: 16,553-16,578.

Yang Z.L., Pitman A.J., McAvaney B., and A. Henderson-Sellers (1995a), The impact of implementing the bare essentials of surface transfer land surface scheme into the BMRC GCM, *Clim. Dyn.*, **11**: 279-297.

Yeh T.C., Wetherald RT, and S. Manabe (1984), The effect of soil moisture on the short-term climatic and hydrologic change: A numerical experiment, *Mon. Wea. Rev.*, **112**: 474-490.

Zeng Q.C., Yuan C.G., Li X., Zhang R.H., Yang F.L., Zhang B.L., Lu P.S., Bi X.Q. and H.J. Wang. (1997), Seasonal and extraseasonal predictions of summer monsoon precipitation by GCMs, *Advances in Atmospheric Sciences*. **14**: 163-176.

Zeng Q.C., Zhang X.H., Liang X.Z., Yuan C.G., and S.F. Chen (1989), Documentation of IAP two-level Atmospheric General Circulation Model, TR044, DOE / ER / 60314-HI, 383 pp.